Christian Pels (Autor)

Ferromagnetic Electrodes for Spin-Polarized Transport - Technology and Experiments

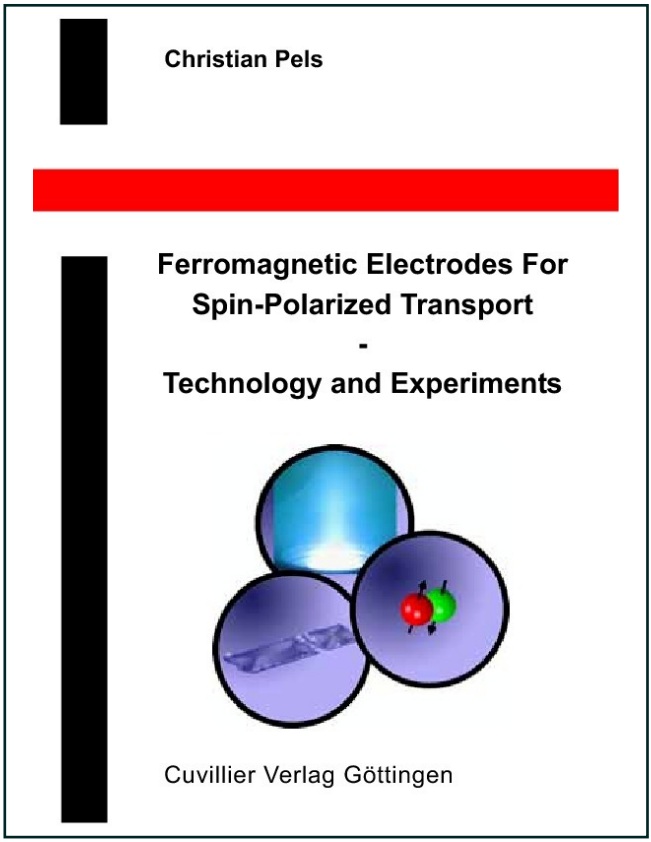

https://cuvillier.de/de/shop/publications/2955

1 Introduction

The era of information technology is marked by the processing and storage of digital data. Data processing has become faster by several orders of magnitude in the last four decades due to the extreme advance in semiconductor technology of large and very large scale integrated (VLSI) circuits. Although Moore's law seems to be valid for roughly another decade, the physical limits, i.e., the energy dissipation via thermal loss in computer processors will put an end to the progress and limit the processing speed. Furthermore, data storage has been improved in a similar way. Ferromagnetic materials are used to write, store and read out digital data, e.g. in hard disc drives. A challenge is the superparamagnetic limit, which means that the information to store is volatile at the moment the size of the storage unit is small enough to allow thermal excitations to destabilize the ferromagnetic state.

Two basic degrees of freedom of the electron are used in today's devices: the electron charge in processors, and the electron spin in storage modules. This leads to the question whether a combination of semiconductor electronics together with spin-polarized electrons extracted from ferromagnets can serve as novel, spintronic devices [Pri95, Aws02]. There are basically two aspects that show the potential of such devices: first, coupling to spin instead of charge in transistor devices could lead to increased switching speed and thus to faster data processing. Second, these devices could serve as non-volatile data storage, i.e., no power supply is required to store the information. This may drastically influence the boot sequence of future computer systems. The theoretical proposal for an electronic analog to the electro-optical modulator [Dat90] can be considered as a pioneering work, and a new research field for semiconductors, now denoted as spintronics, has emerged since 1990. The feasibility of injecting spin-polarized electrons into semiconductors has already been proven with optical [Fie99, Zhu01, Han02, Mot02] and transport experiments [Hu01, Mei02b]. Regarding a complete transistor, it is useful to con-

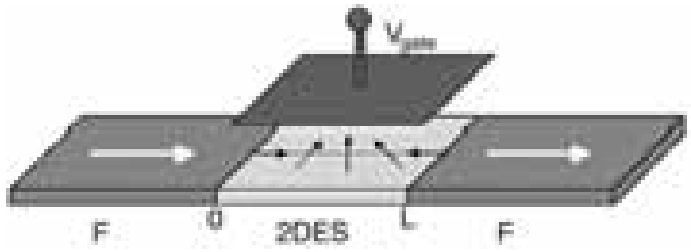

Figure 1.1: Scheme of the Datta and Das transistor [Dat90]. Two ferromagnetic electrodes (F) are adjacent to a two-dimensional electron system (2DES) in the channel of length L. The spin precession is controlled by the gate voltage V_{gate}.

sider several aspects of the device seperately (see Figure 1.1). Ferromagnetic reservoirs F for spin-polarized electrons are necessary, whereby the orientation of the electron spin with respect to the semiconducting channel must be controllable [Mei00, Mei01]. The interfaces between the spin-polarized electrodes and the two-dimensional electron system (2DES) have to be optimized [Gru01a, Gru01b, Hu01, Wun02, Mat02]. The 2DES must be tunable with respect to the spin precession via the gate-controlled Rashba effect [Mat00, Sch02].

The aim of the present work is to develop the deposition technology for ferromagnetic materials which can serve as reservoirs for spin-polarized electrons in hybrid devices. For this, a new magnetron sputter system has been built up for the deposition of ferromagnetic materials. Specific features like long-term data logging and a customized control software are implemented for easy handling and high reproduceability. The influence of the process parameters on the quality of the thin films is investigated systematically using statistical methods, in order to establish reliable processes. The magnetic and electrical properties of homogeneous films and nanostructures are investigated using magnetic-force microscopy (MFM), the magneto-optical Kerr-effect (MOKE), and temperature-dependent resistance measurements. To quantitatively determine the spin polarization of ferromagnetic metals current-voltage characteristics of ferromagnet/superconductor hybrid structures are studied experimentally using lithographically patterned nanostructures and point contacts. A new experimental setup has been developed to investigate these point contacts. Numerical fit procedures have been implemented to allow to extract the electron spin polarization in the ferromagnets.

This thesis is organized as follows: the second chapter gives an introduction to the sputter technology used to deposit ferromagnetic films on semiconductor substrates. The quantitative results of the process characterization are presented. First investigations of the sputter deposited ternary Heusler compound Ni_2MnIn are described. In the third chapter the experimental results of ferromagnetic films and nanostructures are discussed. This includes the results of magnetic-force microscopy applied to permalloy and iron nanostructures, the optical analysis of the anisotropy introduced by the sputter deposition process, and resistance measurements that reveal first quantitative results of the anisotropic magnetoresistance (AMR). The fourth chapter describes the investigations on ferromagnet/superconductor hybrid systems including an introduction to the theoretical concepts. The results of the transport experiments using lithographically defined nanostructures as well as point contacts are presented and compared to data reported in current literature. The thesis ends with a summary in chapter five.

2 Technology

This chapter describes the sputter technology used to deposit iron, permalloy ($Ni_{80}Fe_{20}$), and Ni_2MnIn. First, the basics of sputter processes are briefly reviewed. Then, the sputter system which has been designed and constructed in this work is presented. The third section describes the process characterization, including an introduction to statistical methods for process characterization, and the experimental results.

2.1 Sputter processes

In this section the sputter processes relevant for this work are shortly reviewed and the important process parameters are introduced. For a detailed description of the basics and technical details see [Hof98, Wol90].
Sputter technology is one of the most widely used techniques for deposition and etch processes in semiconductor manufacturing. The method was invented in the 1960s and has been improved consistently for the more and more specific applications of the VLSI era. With respect to industrial applications, the sputter technique provides several advantages compared to alternative methods such as thermal evaporation: the process is much faster and it can be applied to large-area targets, which is crucial for the challenge of depositing thin films with uniform thickness over large wafers of currently 300 mm diameter. Many deposition runs can be accomplished without replacing the target. The deposition rate and the etch rate can be controlled easily by a small number of process parameters. Deposition and etching can be applied in situ. This is already an advantage for VLSI applications, but is essential in hybrid devices investigated in current research, where in particular the specific properties of interfaces between films and substrates are important.
A variety of slightly different processes exists. In this work only two, the dc deposition and the rf etch process are discussed. DC deposition is primarily employed for the deposition of metal films, which serve for various functions in a typical chip: leads, diffusion barriers, etch stops, adhesion, orientation, seed or gate layers. The rf sputter process, originally developed for depositing insulating materials like SiO_2, is now mostly used to clean substrates prior to the film deposition or to etch lateral structures, e.g. to connect the deposited material electrically to a conduction layer buried under the substrate surface.

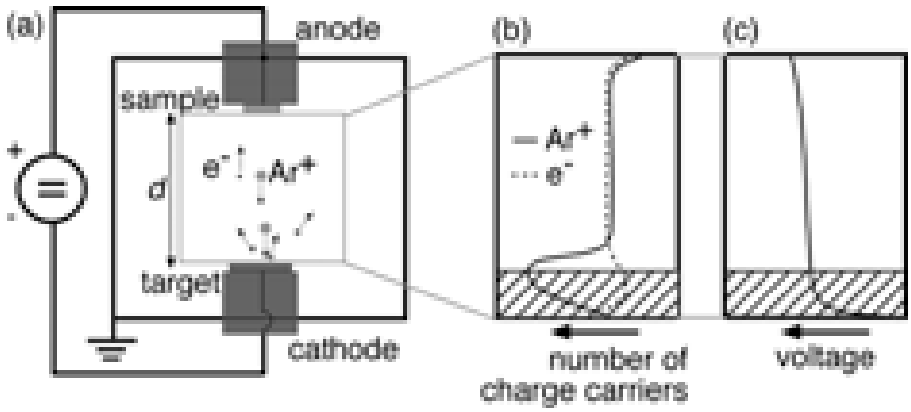

Figure 2.1: (a) Schematic of the dc sputter process. (b) Distribution of the charge carriers. (c) Voltage drop between cathode and anode. The hatched area illustrates the Crookes dark space.

2.1.1 DC magnetron deposition

The basic principles of the dc sputter process can be explained with the setup depicted in Figure 2.1 (a). Consider a vacuum system at a partial argon pressure p_{process} with two electrodes spaced at a distance d, the anode carrying the sample and the cathode carrying the target. If a high voltage V is applied between anode and cathode at the start of the process, a free electron will be accelerated by the electric field $E = V/d$ and therefore collect kinetic energy. It collides with an argon atom after having travelled the mean free path λ, which is proportional to the reciprocal pressure. At p_{process} = 0.01 mbar λ is of the order of 1 cm. With $d = 15$ cm and $V = 300$ V the electron gains a kinetic energy of $E_{\text{kin}} = 20$ eV while moving along the distance λ. Most of the collisions are elastic, so that the electron keeps its energy. An inelastic collision with an argon atom leads either to excitation or ionization of the atom, depending on the transferred energy. For argon, the excitation energy is 11.5 eV, and the ionization energy is 15.7 eV. While excitation causes light emission, ionization creates a new free electron and an argon ion. Subsequently, the electron is accelerated again, and a cascading effect begins, which leads to a breakdown of the discharge rapidly. A current regulation supplying the cathode with electrons and collecting electrons at the anode can maintain the discharge. As the system now contains equal numbers of positive and negative charge carriers it is referred to as a plasma. The dynamics of current transport in such a plasma are complicated. In equilibrium, i.e., when a constant current flows, the plasma has a distinct structure. Figures 2.1 (b) and (c) show the most important characteristics of this structure. The light electrons are rapidly accelerated away from the target, while the heavier argon ions move slowly and thus remain longer in this region. The positive excess charge in this area (Figure 2.1 (b)) causes the major voltage drop between cathode and sample (Figure 2.1 (c)). The resulting electric field is stronger than in the rest of the plasma, so that electrons are more likely to ionize argon atoms than to excite them. Therefore, this region is called (the Crookes) dark space. Here, the argon ions are rapidly accelerated in the direction of the target. They undergo further collisions on their way towards the target, so that the energy distribution of the particles finally impacting on the target is broadened. The

geometry and the properties of the electrical potential in this region mainly govern the sputter process. As the geometry of the system is fixed, the only variable parameters are the pressure p_{process} and the electrical potential, which is mostly parameterized by the dc power P_{dc} of the plasma. This also determines the kinetic energy of the argon ions, which lies in the range of 100 eV to 10 keV for common sputter systems. This is sufficient to dislodge atoms from the target. Being neutral particles, these can spread out isotropically in the chamber, in particular, they form a thin film on the sample. The number of sputtered atoms per incident particle is denoted as sputter yield. The energy of the sputtered atoms lies in the range of 10 to 40 eV, depending on the target material and the applied dc power P_{dc}. It is reduced by collisions of the sputtered atoms with argon atoms or ions and electrons, respectively. At a fixed distance between target and sample, this diffusion behavior is again determined by the process pressure p_{process} and the dc power P_{dc} only. Therefore, these two parameters influence the growth properties.
The efficiency of the process is increased by the use of magnetron cathodes. Here, a specific configuration of permanent magnets is located below the target creating a magnetic field B above the target. The combination of E and B forces the electrons onto closed paths, so that each electron causes several ionizations before it escapes from the dark space [Ros87]. The particular case of ferromagnetic targets requires magnets with strong stray fields to compensate for the shielding effect of the highly permeable target itself (see Section 2.2).

2.1.2 RF etching

The schematic of a rf plasma process is illustrated in Figure 2.2 (a). Again, a vacuum system at a partial argon pressure p_{process} is considered. If an ac voltage is applied between cathode and anode instead of a dc voltage, a plasma forms oscillating with the ac frequency[1]. Electrons pick up energy from this oscillation causing either excitation or ionization of argon atoms like in the dc plasma. Because the electrons move much faster than the argon ions, a certain number of electrons are collected from the anode after one half of the oscillation cycle, while much less argon ions are neutralized at the cathode. This causes a net current and a net dc bias voltage V_{dcbias} between the electrodes in this half of the cycle. After a few oscillations the bias voltage drifts to an equilibrium state resulting in a net movement of the inert argon ions in the direction of the cathode. Due to the ac character of the plasma the direction of the bias voltage drop depends on the electrical coupling of the rf power supply to the electrodes. In principal, sputtering from the target is possible as well as sputtering from the sample surface, which is then called etching. In the latter case, the sample is the cathode, i.e., it is capacitively coupled to the rf power supply via an impedance matching network (matchbox). A grounded shielding acts as anode as depicted in Figure 2.2 (b). In rf discharges, the plasma dynamics are more complex than for dc discharges and not understood in all details [Hof98]. The most important regions of the discharge are the plasma boundaries, known as sheaths. In these regions the quasi-neutrality

[1] In most systems, a frequency of 13.56 MHz is used. This number lies in the radio frequency range, which explains the notation rf sputtering, and it is one of the frequencies approved by the regulations of international communication authorities.

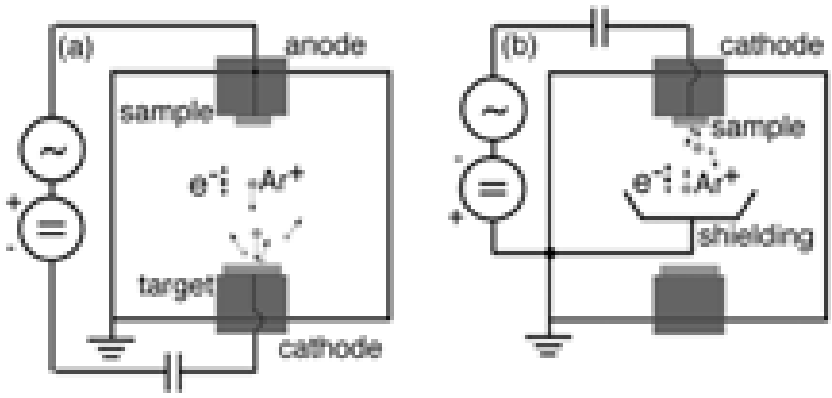

Figure 2.2: (a) Schematic of the rf sputter process. (b) Configuration for the rf etch process. In this case, the sample electrode serves as cathode.

of the plasma does not hold, and ions are accelerated. In an etch process, the sheath region between the plasma and the sample is crucial. In many configurations, the ion bombardment results in mechanisms that allow lithographic patterns to be etched anisotropically with little or no lateral removal of material. The ion energies lie in the range of 50 eV to 1 keV. Similar to the dc sputter process, the relevant process parameters are the pressure p_{process} and the ion energy, which in this case is parameterized by the dc bias voltage V_{dcbias}.

2.2 UHV sputter system

In this work a UHV sputter system for ferromagnetic materials has been developed. The system is designed for a dc sputter process with an in situ rf etch step prior to the deposition. Additionally, it contains a transfer chamber which allows fast process cycles. The setup is shown in Figure 2.3. Table 2.1 gives an overview of its technical components.
The system consists of two chambers, the process chamber and the transfer chamber, which are pumped seperately with standard turbomolecular and rotary pumps. The base pressure in the process chamber p_{base} lies in the 10^{-9} mbar range. The pressure measurement is performed with a combined pirani/cold cathode gauge. During the process, a capacitance sensor is used. Before and after the deposition process, the residual gas composition is analyzed by a mass spectrometer.
The sample holder is located at the top of the chamber. Its lower part consists of a water cooled copper inset, which is in direct thermal and electrical contact with a removable copper plate carrying the sample. The electrical connection of the sample can be manipulated from outside. For the deposition, the sample is connected to ground, during the etch process, the sample is connected to the output of the rf power supply which includes the impedance matching network. The cathode is located at the bottom of the chamber (see inset of Figure 2.3). Its upper part is a water-cooled copper plate carrying the target. The target edge is cylindrically shielded to avoid sputtering of non-target atoms from the cathode body. The target is electrically connected to the output of the dc power supply. The NdFeB magnetron magnets are adjustable from outside

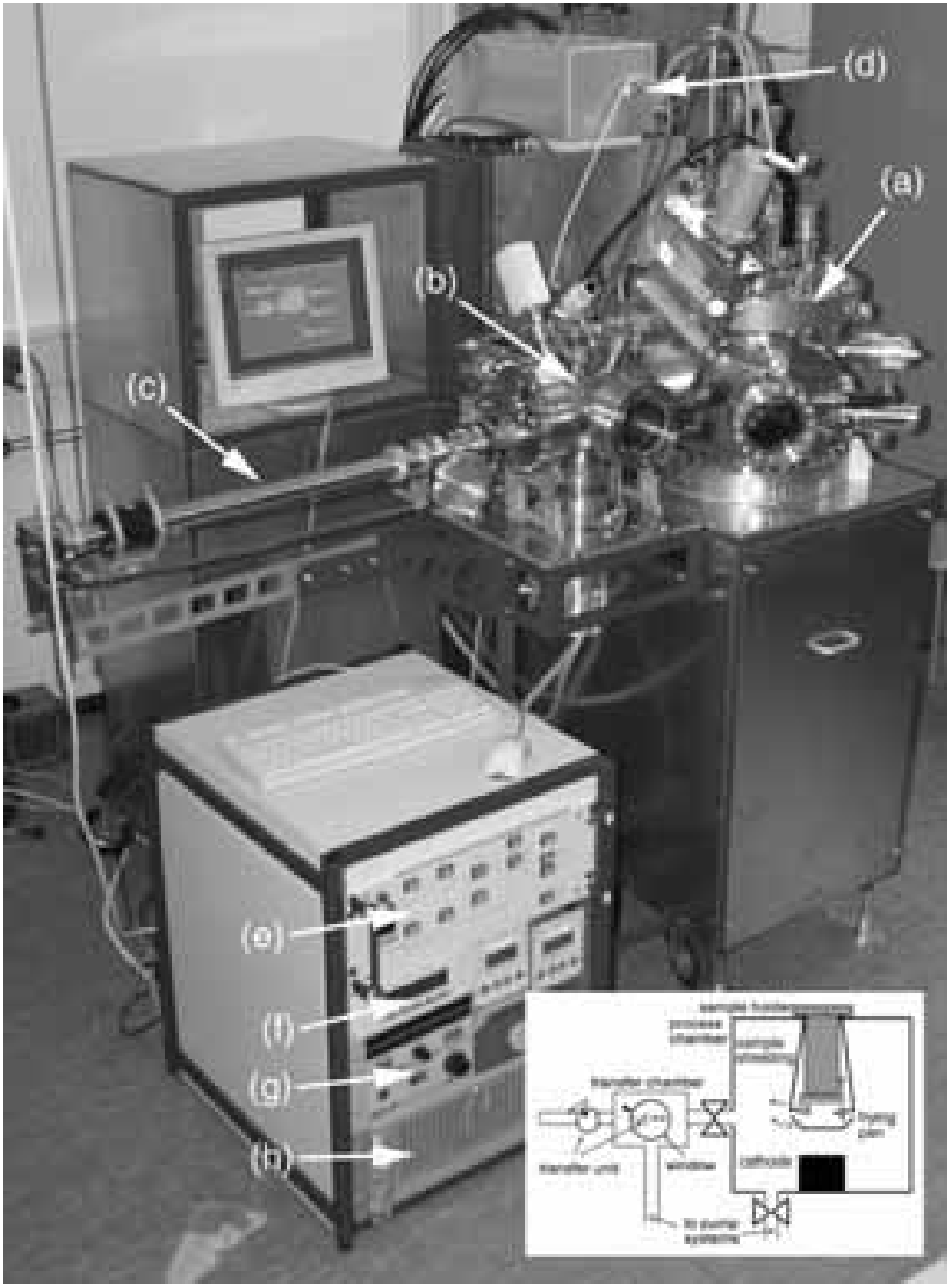

Figure 2.3: Photograph of the UHV sputter system for ferromagnetic materials. The inset shows a schematic of the system. (a) Process chamber, (b) Transfer chamber, (c) Transfer unit, (d) Matchbox, (e) Main electronics, (f) Pump and vacuum sensor readout, (g) DC and ac power supplies, (h) Process control computer.

vacuum setup	turbomolecular pumps	Pfeiffer Vacuum TMH 521 Pfeiffer Vacuum TMP 071P
	rotary pumps	Pfeiffer Vacuum DUO 030 A Pfeiffer Vacuum DUO 5
residual gas analysis	full range pressure measurement prevacuum pressure measurement process pressure measurement	Pfeiffer Vacuum PBR 260 Pfeiffer Vacuum TPR 265 Pfeiffer Vacuum CMR 274
	mass spectroscopy	Inficon Transpector 2 C100M Transpectorware 3.40
power supply	dc power supply rf power supply rf matching network	Advanced Energy MDX-1.5K Hüttinger PFG 300 RF Hüttinger PFM 1500 A
cathode	UHV sputter source	Kurt J. Lesker TM03U
remote control	hardware	AMD Athlon 1600+, RS 232, RS 485 Arcom APCI-ADADIO converter
	software	Windows NT 4.0, LabView 6.1, customized process control software

Table 2.1: Technical components of the UHV sputter system for ferromagnetic materials.

and must be completely removed for the bakeout of the chamber. The magnets are shown in Figure 2.4 (a). The combination of one central magnet (e.g. north pole aligned to the top) surrounded by a circular configuration of south pole magnets generates a toroidal field, which confines the electrons above the target. Due to the shielding effect of the ferromagnetic target its thickness is limited. This effect is depicted in Figures 2.4 (b) and (c). In the present system, the target thicknesses are 1.2 mm for iron, 2.0 mm for permalloy ($Ni_{80}Fe_{20}$), and 5.0 mm for Ni_2MnIn. Figure 2.4 (b) shows a finite element simulation of the magnetic field above the target for a non-magnetic (left) and magnetic iron target (right) in arbitrary units (picture taken from [GEN02]). The orientation of the magnetic field is illustrated by the lines, and the gray level symbolizes the field strength. The diagram depicts the confinement of the magnetron field due to the ferromagnetic iron target resulting in lower field strengths in comparison with the case of a non-magnetic target. Figure 2.4 (c) shows field strengths measured with a Hall magnetometer for the cathode used in the present system for non-magnetic (left) and magnetic iron target (right). They show the shielding effect of the target quantitatively. The sign reversal between the center and the edge data indicates the pole configuration mentioned above. At a distance of 10 cm above the cathode the magnetic field strength has decreased to the order of 1 mT.
The sample preparation begins with venting the transfer chamber and inserting the sample which is fixed on a copper plate with a conducting silver emulsion. After pumping the transfer chamber for approximately one hour ($p_{\text{transfer}} < 10^{-6}$mbar) the valve between transfer chamber and process chamber is opened and the sample is transferred into the sample holder of the process chamber with mechanical UHV actuators. After closing the valve the residual gas composition is analyzed by mass spectroscopy. Next, the orifice of the evacuation tube is reduced via the